6

Retrospective image correction in the presence of non linear temporal magnetic field changes using multi-channel navigator echoes

M.J. Versluis
B.P. Sutton
P.W. de Bruin
P. Börnert
A.G. Webb
M.J. van Osch

Magnetic Resonance in Medicine 2012;68(6):1836-1845

ABSTRACT

Spatio-temporal magnetic field changes in the brain caused by breathing or body movements can lead to image artifacts. This is especially a problem in T_2^*-weighted sequences. With the acquisition of an extra echo (navigator) it is possible to measure the magnetic field change induced frequency offset for a given slice during image acquisition. However, substantial local variation across a slice can occur. This work describes an extension of the conventional navigator technique that improves the estimation of the magnetic field distribution in the brain during strong field fluctuations. This is done using the combination of signals from multiple coil elements, the coil sensitivity profiles and frequency encoding; termed sensitivity encoded (SENSE) navigator echoes. In vivo validation was performed in subjects who performed normal breathing, nose touching and deep breathing during scanning. The SENSE navigator technique leads to an error reduction in estimating the field distribution in the brain of 73 ± 16% compared to 56 ± 14% for conventional estimation. Image quality can be improved via incorporating this navigator information appropriately into the image reconstruction. When the SENSE navigator technique was applied to a T_2^*-weighted sequence at 7 Tesla a ghosting reduction of 47 ± 13% was measured during nose touching experiments compared to no correction.

INTRODUCTION

Magnetic resonance imaging (MRI) is ideally performed in a spatially and temporally stable and homogeneous magnetic field, especially when using gradient echo sequences in which magnetic field inhomogeneities lead to loss of phase coherence. It has been shown previously that body movements and respiration lead to substantial variations of the magnetic field in the brain (1–6). These effects are significantly more pronounced at high magnetic field strengths. One of the sequences frequently used at 7 Tesla is a strongly T_2^*-weighted gradient echo, because of the high intrinsic contrast in both magnitude and phase which allows differentiation of cortical layers, as well as detection of diffuse depositions of iron associated with various neurodegenerative diseases (7–10). Due to the sensitivity of this sequence to spatial and temporal variations in both T_2^* and phase (through changes in the resonance frequency), changes in these parameters that are not related to tissue properties can have a large detrimental effect on image quality.

Variations in the local magnetic field can be separated into static inhomogeneities, i.e. those that remain constant during the experiment, and dynamic inhomogeneities, i.e. those that fluctuate throughout the experiment. On most current systems up-to-third order shimming is available to compensate at least partially for static inhomogeneities. In contrast, dynamic magnetic field changes, such as caused by respiration and body movements cannot be corrected using static shimming approaches.

Several methods, either prospective or retrospective, exist to measure and correct partially for these dynamic field variations. It has been shown that a reference scan can be used to relate field changes caused by normal respiration to the chest motion (1). By measuring the chest motion during image acquisition prospective correction was possible by dynamically switching the shim values. Using this approach, however, only periodic field fluctuations due to respiration can be corrected while non-periodic fluctuations due to cardiac pulsations and body movements, for example, lead to fluctuations that are not corrected. Others have used external magnetic field probes to sample the magnetic field changes at several spatial locations during image acquisition, an approach that is also capable of measuring non-periodic fluctuations, but requires dedicated hardware (11, 12).

Another approach to compensate for dynamic field variations is to sample an extra navigator echo before phase encoding (6, 13–17), or to use special sequences capable of self-navigation (18–20). Based on the difference between successive navigator signals the temporal magnetic field disturbance can be

estimated and corrected during image reconstruction. An advantage of the navigator echo approach is that it does not require dedicated hardware. So far this technique has mostly been used to correct for zeroth order temporal changes in the magnetic field. This can be sufficient to correct for magnetic field changes induced by normal respiration when axial images through the brain are considered (2, 4). Substantial improvements in image quality of high resolution T_2^*-weighted images have been shown in Alzheimer's disease patients, where the changes in the magnetic field were measured for each axial slice separately and used to correct the phase of each acquired k-space line retrospectively (6). However, residual image artifacts still remain, which were hypothesized to arise from spatio-temporal magnetic field fluctuations *within* a slice.

The aim of this work is to address and correct for the artifacts that are caused by these within-slice dynamic magnetic field fluctuations. A prerequisite for this approach is that information about the magnetic field distribution must be available at a sufficiently high temporal and spatial resolution. In this work the field map information is derived by integrating frequency-encoded navigators with the intrinsic spatial information from the coil sensitivity profiles of the individual elements of the receive array (21–23). Subsequently this information was used to correct retrospectively the corrupted images. To test the robustness of this correction approach strong spatio-temporal magnetic field inhomogeneities were produced by having subjects perform nose touching and deep breathing tasks during image acquisition. This was used to model the worst case fluctuations that can occur during patient examinations. Additionally, the method was evaluated in cooperative subjects instructed to remain still and breathe normally.

MATERIALS AND METHODS

All experiments were performed on a 7 T whole body system (Philips Healthcare, Best, The Netherlands), equipped with a quadrature transmit and 32-channel phased array head coil (Nova Medical, USA). All subjects gave written informed consent prior to the study in compliance with local ethics regulations.

This study is divided into two parts, in the first part the accuracy of the spatial field estimations is investigated using very fast imaging as a ground truth. In the second part a reconstruction framework is developed to correct retrospectively the data using the measured dynamic field fluctuation information.

Spatial field estimations

The navigator echo was acquired immediately after each RF excitation using 32 receive channels; see Figure 1 for more details. A complex difference signal was calculated between the first and the successively acquired navigator echoes, which is subsequently converted to a frequency shift for each channel ($f_{0,nav}$). The navigator echo was acquired once for every excitation, and a phase correction was applied to all k-space lines following the same excitation, either one gradient echo, or the entire echo planar imaging (EPI) train.

Four different methods were investigated for spatial field mapping based on this one-dimensional navigator. The first method consists of a complex summation over the individual channels and temporal sampling points, resulting in a global estimation of the frequency shifts: this is the zeroth order approach outlined in ref. (6) and is used as a reference. The second method consists of a coil sensitivity weighted summation over the channels and summation over all temporal sampling points: this is termed the sensitivity encoded (SENSE) navigator approach. The third method is similar to the second method but in addition includes the spatial information of the frequency encoding gradient in the anterior/ posterior direction: this is termed the frequency encoded SENSE navigator. The fourth method includes the frequency encoding gradient after averaging all channels, this is called the frequency encoded navigator.

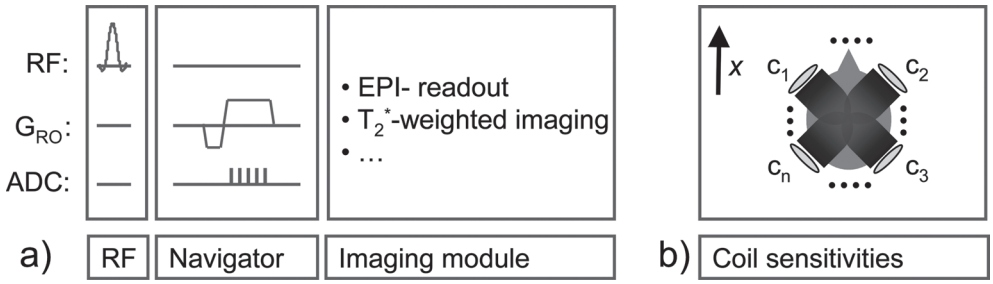

Figure 1: SENSE navigator sequence details.
(a) The acquisition of the navigator is shown schematically in a sequence diagram. The navigator echo is acquired after slice selection prior to phase encoding and is followed by an imaging module. G_{RO} is the navigator readout gradient, and ADC is the analog-to-digital converter. (b) Multiple coil elements with different coil sensitivities are used to sample the navigator echo simultaneously (depicted schematically as $c_1 - c_n$). Four different navigators have been studied. In the first a complex summation of all temporal sampling points is performed and all coil signals are simply added before evaluation. Also in the second the sampling points are summed, but all coil signals are added including spatial coil sensitivity weighing, while the third is equal to the second one, but taking into account the spatial frequency encoding gradient (G_{RO}) along the ***x*** direction to increase the spatial definition. The fourth approach only uses the G_{RO} after adding all individual coil signals.

All four types of field map reconstruction (zeroth order, frequency encoded

and both SENSE navigator estimations) use exactly the same acquired data, allowing the results for the different approaches to be compared.

For the SENSE navigator field techniques the individual field estimations ($f_{0,nav}$) were weighted according to a separately acquired coil sensitivity map (CSM) that describes the spatially varying sensitivity of each receive coil element, to produce a dynamic low resolution two dimensional field distribution map ($f_{0,nav}(x,y,t)$) (22):

$$f_{0,nav}(x,y,t) = \sum_{ch} f_{0,nav}(x,t,ch) \cdot CSM(x,y,ch) \qquad [1]$$

Where *x* and *y* are the frequency- and phase encoding directions, respectively and *ch* denotes the receive coil element. The *CSM* was calculated on the scanner using a manufacturer provided method that uses the ratio between an image acquired with the 32 channel receive array and the quadrature transmit-receive coil as receive coil in order to limit the effect of T_2 differences on the CSM.

The amplitudes of the CSMs are normalized voxelwise such that each voxel location, when summed over the channels, adds up to unity. For the frequency encoded SENSE navigator, first a Fourier transform was applied along this direction to resolve the spatial dependence. The phase difference signal in the frequency encoding direction was fitted using a polynomial of 2nd order to reduce the effects of noise, after which the previously described steps were performed. This was empirically found to be the lowest polynomial order that matched the observed magnetic field distribution patterns adequately. For the SENSE navigator $f_{0,nav}(x, t, ch)$ reduces to $f_{0,nav}(t, ch)$ and for the frequency encoded navigator to $f_{0,nav}(x, t)$. The zeroth order navigator results in a single frequency change value for each time point: $f_{0,nav}(t)$.

To estimate and assess the accuracy of these four navigator-based field estimations the following experiment was conducted. A fast single shot EPI sequence was run with the following parameters: repetition time (TR) /echo time (TE)/flip angle (FA) = 65 ms/ 25 ms/ 25°, EPI factor = 27, SENSE factor 2.3, voxel size = 3.3x3.3x3 mm^3, bandwidth per pixel = 23 Hz. Before image acquisition the navigator echo was acquired using 32 coil elements at TE_{nav}=2.1 ms. A total of 4000 images were acquired resulting in 4'20'' scanning time. Four subjects performed the following tasks during scanning: touching their nose, moving one arm, touching their neck, and taking deep breaths. The first image was taken as a reference and the phase difference with respect to

subsequent images was calculated. These measurements were considered the ground truth and were compared to the navigator based estimations of the spatio-temporal field variations. Head motion was minimized using foam padding and was visually monitored.

To assess the error for each of the three approaches sum-of-square difference (SSD) maps were generated between the ground truth measurements and the navigator based estimations. The maps were summed over all voxels and timepoints to yield a single number indicating the accuracy of the specific navigator approach. A reduction in the SSD (RSSD), defined as ($SSD_{navigator}$ – $SSD_{no\ correction}$) / $SSD_{no\ correction}$ will be reported.

Image artifact correction

The second component of the study consists of using the different navigator field estimation approaches for image artifact correction in a T_2^*-weighted sequence. The following sequence was used to demonstrate the effects that magnetic field variations can have on image quality. Six subjects were scanned using a 2D gradient echo sequence with the following parameters: TR/TE/FA = 400 ms/20 ms/ 30°, the navigator was acquired at TE_{nav}=10 ms, voxel size 0.42x0.42x3 mm^3, and data matrix size of 480x480. Three separate scans were acquired: 1) subject lying still, 2) subject touching nose at approximately 10 s intervals, and 3) subject taking deep breaths. The first scan is considered as a reference image and is used to compare the performance of the navigator based reconstructions of images acquired during intentional magnetic field variations. For each acquired k-space line an estimation of the magnetic field change was made using the previously described navigator techniques. The resulting phase errors can be incorporated in the image encoding equation (11, 24), written in matrix form:

$$\mathbf{k} = \mathbf{E}\,\mathbf{m} \qquad [2]$$

Where k is the k-space data, m is the image space data, both stored as a column vector of size $[N_x N_y]$, where N_x is the number of frequency encodings and N_y is the number of phase encodings, or voxels along the respective dimensions. E is the encoding matrix, containing both the Fourier encoding terms as well as the derived phase errors for each shot and location. If parallel imaging is not considered E is of size $[N_x N_y \times N_x N_y]$ and becomes prohibitively large even for moderate imaging resolutions. Therefore an iterative approach based on a conjugate gradient solver was used that calculates only the relevant parts of E and the complex conjugate E^H to solve this problem efficiently (24–26). Equation 2 can be rewritten as:

$$\mathbf{k} = \sum_{i} \{[\mathbf{M}_i \, \mathbf{F} \, \mathbf{P}_i] \, \mathbf{m}\} \quad \textbf{[3a]}$$

and,

$$\mathbf{k} = \sum_{i} \left\{\left[\mathbf{P}_i^{H} \, \mathbf{F}^{-1} \, \mathbf{M}_i^{H}\right] \mathbf{m}\right\} \quad \textbf{[3b]}$$

Where equation 3a calculates **E m** and equation 3b calculates $\mathbf{E}^{H}\,\mathbf{m}$. M_i is a diagonal matrix of size [$N_x N_y$ x $N_x N_y$] that selects the data for the i^{th} shot. F is the Fourier transformation, F^{-1} is the inverse Fourier transformation and P_i is a diagonal matrix of size [$N_x N_y$ x $N_x N_y$] that contains the phase variations for the i^{th} shot. The summation is performed over the number of shots. Based on visual inspection the maximum number of iterations was set to 3, to limit reconstruction times. Data for multiple coils were reconstructed separately and combined using the coil sensitivity maps (27). Images were reconstructed both with and without navigator echo correction. Phase images were unwrapped using k-space based high-pass filtering, as detailed in ref. (28)

Overall reconstruction times were 1 minute per channel for a single slice on an 8 core Intel 2.27 GHz processor with 12 GB internal memory, using Matlab 2009a (Mathworks, USA)..

To assess image quality, difference images were generated between the separately acquired non-corrupted image (where the subject was asked to lie still in the scanner) and the images where movements were intentionally made. A large percentage reduction in the difference image corresponds to a small difference between the reference image and the retrospectively corrected image, which is a measure for how well the navigator reconstruction performed. In four subjects the reference scan was repeated while the subject was lying still, in order to assess the stability of the navigator based approaches with respect to very small magnetic field fluctuations.

RESULTS

Figure 2 is an example of a single time frame of the spatial magnetic field distribution and illustrates the performance of the different approaches during touching of the nose. Figure 2a displays the “ground truth” magnetic field distribution. The corresponding estimated field change maps using the navigator echo based approaches are shown in Figure 2b for zeroth order, Figure 2c for SENSE navigator estimation without frequency encoding, 2d for frequency encoded navigator estimation and in 2e for SENSE navigator estimation with frequency encoding information. In Figure 2a a spatially inhomogeneous magnetic field distribution is observed with a spread of up to

20 Hz between the anterior and posterior regions. The zeroth order navigator measured a global frequency offset of -6.5 Hz, approximately the average frequency offset over the entire slice. Visually it can be appreciated that both SENSE navigator approaches and the frequency encoded estimation lead to an improved field estimation compared to the zeroth order technique. The low bandwidth of the EPI sequence leads to geometric distortions on the order of 1 to 2 pixels in the phase encoding direction for the observed field variations during the nose touching experiments.

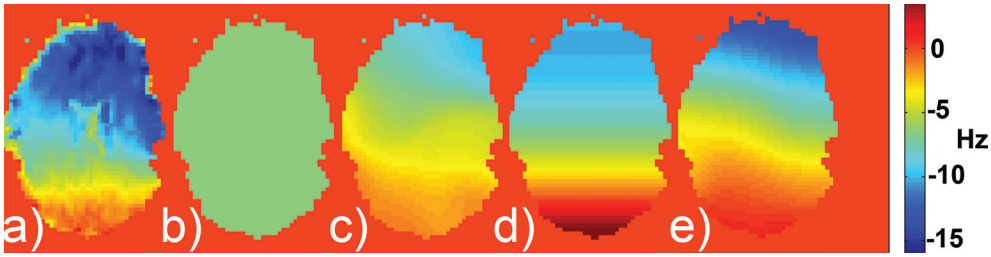

Figure 2: Magnetic field changes during nose touching.
Field changes in an axial brain slice during nose touching measured using an EPI sequence (a) which is considered to be the ground truth field change measurement. b-e) show the navigator based field change estimations. b) is the result of the conventional zeroth order navigator, a global frequency offset of -6.5 Hz is estimated for the entire slice with no spatial resolution. c) is estimated using the SENSE navigator. (d) is estimated using only frequency encoding, and (e) is estimated using the frequency encoded SENSE navigator. The magnetic field varies substantially over the slice between -20 Hz frontally to +5 Hz posterior. Table 1 shows a quantitative summary of the results.

To assess the accuracy of the different approaches quantitatively, SSD maps are generated over the complete time course. The RSSD for the different navigator estimations compared to no estimation is calculated. The zeroth order navigator results in a reduction of 56 ± 14% ($p = 0.02$). Further reductions are found for SENSE navigator estimation: 70 ± 14% ($p = 0.02$), for the frequency encoded navigator estimation: 70 ± 16 % ($p=0.02$) and 73 ± 16% ($p = 0.02$) is found for the frequency encoded SENSE navigator estimation (see table 1 for details).

Table 1: Reduction in sum of squared difference (RSSD) values.	
Zeroth order navigator	56 ± 14% †
SENSE navigator (no FE)	70 ± 14% †,‡
FE navigator	70 ± 16 % †,‡
SENSE navigator (with FE)	73 ± 16% †,‡

RSSD values for each navigator echo based approach compared to no navigator correction. (no FE): no frequency encoding gradient information is used; (with FE): frequency encoding information of the navigator echo is used. P-values are calculated using a paired t-test, comparing RSSD values between no correction and the different navigator techniques. † denotes significantly different from no correction; ‡ denotes significantly different from zeroth order navigator correction, $p<0.05$.

The application of the navigator based field estimations for retrospective image correction is shown in Figure 3. Images from the T_2^*-weighted sequence are shown for two slice locations in the brain during nose touching at an interval of approximately 10 s. Figures 3a and 3f show the results when no correction is applied. Severe image artifacts are observed, resulting from the strong dynamically varying magnetic field changes during acquisition. When the image is corrected using a single phase offset for each acquired k-space line (Figures 3b and 3g, zeroth order correction) the image quality is improved, but artifacts still remain. When coil-based SENSE navigator correction is applied image quality is further improved. Figures 3c and 3h show the corresponding results for SENSE navigator correction. Figures 3d and 3i show the resulting images for the frequency encoded navigator correction and Figures 3e and 3j show the results for frequency encoded SENSE navigator correction. Most image quality improvements are observed in the anterior part of the brain. Visually the best image quality is obtained for frequency encoded navigator field estimation and frequency encoded SENSE navigator estimation. The bottom row shows the difference images compared to an artifact free image when no intentional subject motion was introduced. A reduction of differences is visible when navigator correction is applied. Histograms of the difference image values are shown in Figure 3 as an inset on the difference maps. The histograms corresponding to the SENSE and frequency encoded navigator corrected data show a narrower distribution compared to no correction, or zeroth order correction histograms.

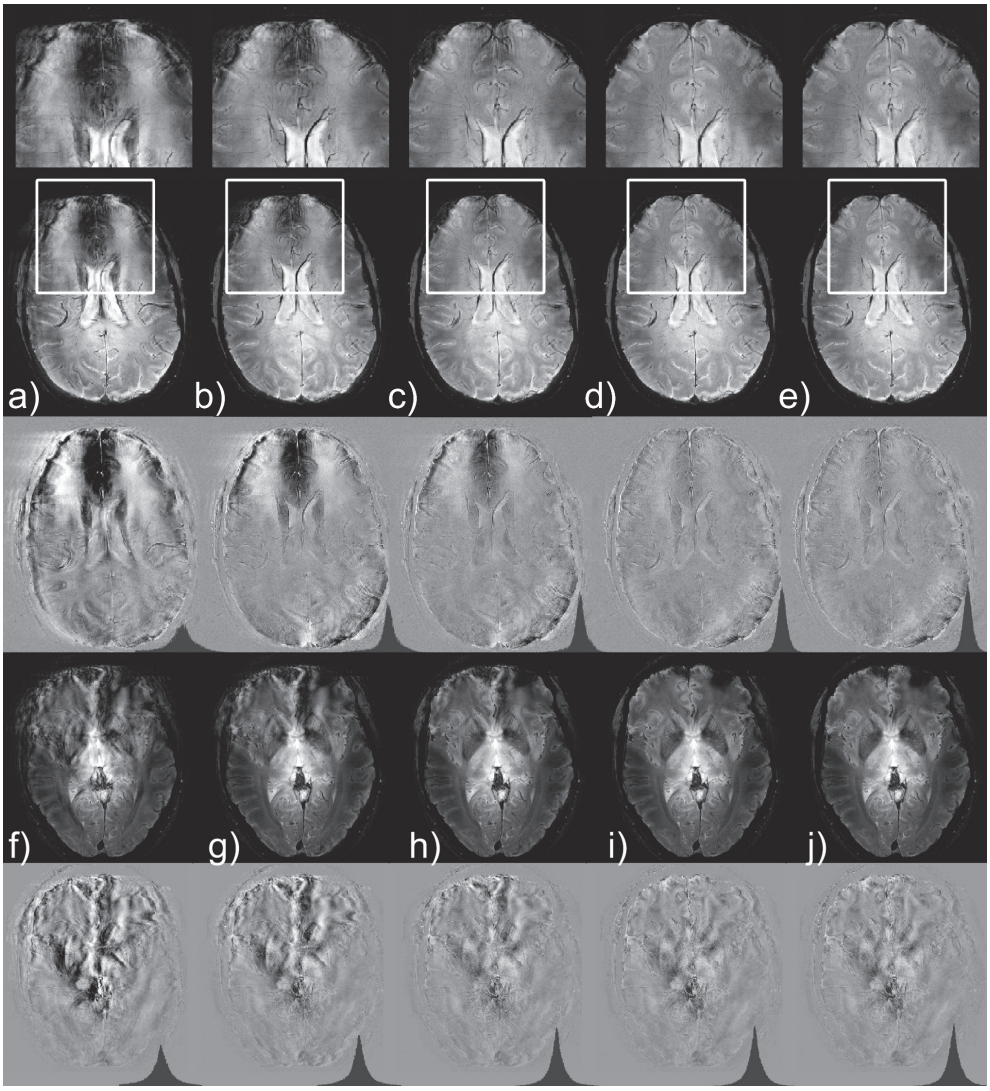

Figure 3: Navigator corrected T_2*-weighted imaging during nose touching.
Different reconstructions are shown for two slice locations in the brain (a-e) and (f-j), respectively, Below each image the difference image is shown between the corresponding reconstructions and an artifact-free image (no nose touching). Histograms of the difference values are displayed as an inset in the bottom left corner of the difference images. a,f) the original dataset without correction. b,g) Image corrected using conventional (zeroth order) navigator correction. Artifacts in the frontal part of the brain are reduced (see zoomed in sections), c, h) image after SENSE navigator correction. d, i) Image using the frequency encoded navigator correction, without using coil sensitivity information, e, j) image after frequency encoded SENSE navigator reconstruction., The histograms of the difference values show that the distribution of values becomes narrower when navigator correction is applied. Results are summarized in table 2

With the proposed reconstruction methods the complex MRI signal is preserved and therefore both magnitude and phase images can be reconstructed. Unwrapped phase images for a single subject are shown in Figure 4 during a nose touching experiment. The image quality improves when navigator correction is applied (Figures 4a – e), with the most pronounced reduction in image artifacts for frequency encoded SENSE navigator correction. In addition improved phase unwrapping is observed, depicted by the arrow in the zoomed in sections of the anterior part of the brain. This is particularly apparent in Figures 4d and 4e.

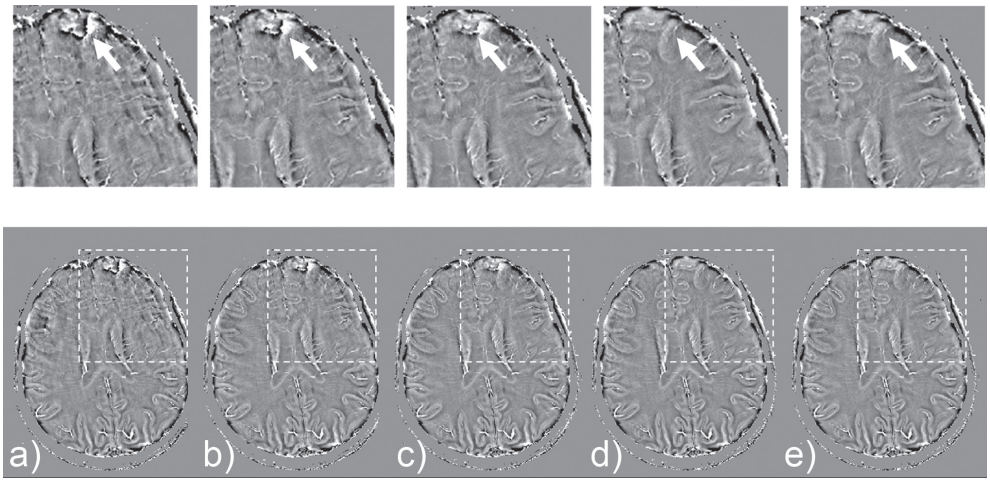

Figure 4: Navigator corrected phase images during nose touching.
Unwrapped phase images during nose touching. a) no correction, b) zeroth order correction, c) SENSE navigator correction, d) frequency encoded navigator correction and e) frequency encoded SENSE navigator correction. Similar to the results of figure 3 much improved image quality is visible for the frequency encoded and SENSE navigator approaches, resulting in clearer phase images. Phase images were unwrapped using a homodyne high-pass filter with a kernel size of 80. The top row shows a zoomed section of the anterior part outlined by the white box. The arrow points to an area that significantly improves. Images are scaled between $-\pi/5$ and $\pi/5$.

Figure 5 shows images of a different subject while performing deep breathing. Again the best results are obtained for frequency encoded and SENSE navigator correction, however in this case the improvements compared to the other approaches are less pronounced. The middle row shows a zoomed section of the posterior part, the arrow points to one of the artifacts that is resolved only when SENSE navigator correction is applied. The bottom row shows the difference images compared to an artifact free image. The difference images are scaled differently compared to Figure 3. Histograms of the difference images show a narrower distribution of values when navigator correction is applied compared to no correction. The differences in histo-

grams between the zeroth order correction and other navigator techniques are less pronounced.

Table 2: Reduction in difference images comparing the navigator approaches.

	0th order correction	SENSE navigator	Frequency encoded navigator	Frequency encoded SENSE navigator
Nose touching	22 ± 9% †	36 ± 13% †,‡	46 ± 14% †,‡	47 ± 13% †,‡
Deep breathing	11 ± 12%	13 ± 12% †,‡	14 ± 12% †,‡	15 ± 12% †,‡
Normal breathing	15 ± 14%	15 ± 14%	15 ± 15%	15 ± 15%

Percentage reduction in difference between image acquired when subjects (n=6) were lying still and when subjects were performing nose touching, deep breathing or normal breathing for the different navigator correction approaches. P-values are calculated using a paired t-test, comparing absolute SSD maps between the artifact free image and the different navigator techniques. † denotes significantly different from no correction; ‡ denotes significantly different from zeroth order navigator correction; $p<0.05$.

The improvement in image quality was quantified by taking the difference between the corrupted image of a single slice and the separately acquired reference image when the subject was asked to lie still in the scanner. A percentage reduction in the difference image of up to 47 ± 13% ($p = 0.01$) is obtained for nose touching experiments and up to 15 ± 12% ($p = 0.04$) for the experiments consisting of deep breathing (see table 2 for details). When no artificial field fluctuations were introduced navigator correction resulted in a reduction in the amount of differences of 15 ± 14 % ($p=0.08$), irrespective of the navigator correction technique used, compared to when no correction is performed.

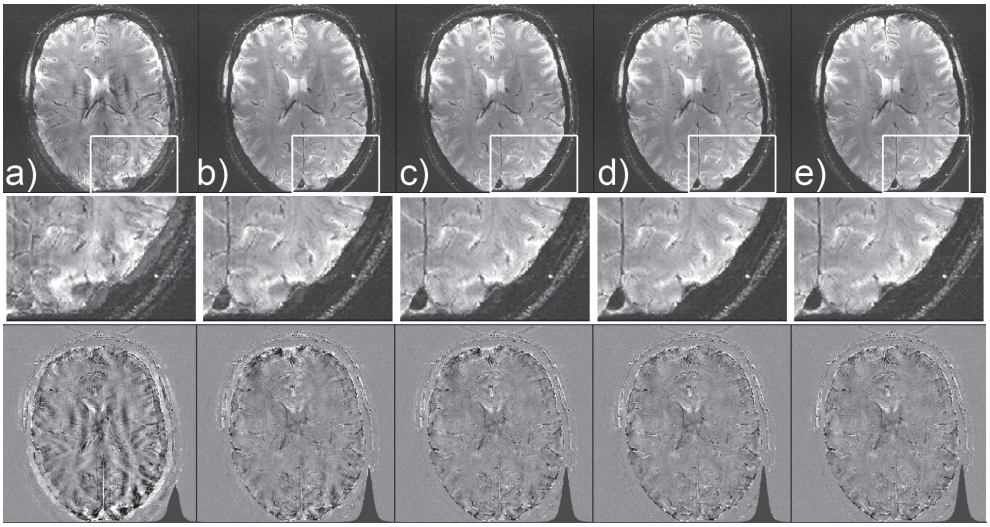

Figure 5: Navigator corrected T_2*-weighted imaging during deep breathing.
Different reconstructions are shown. a) Uncorrected image, b) image using zero order correction, c) using SENSE navigator correction, d) using frequency encoded correction and e) using frequency encoded SENSE navigator correction. The bottom row shows difference images between the corresponding reconstructions and an artifact-free image. Histograms of the difference values are displayed as an inset in the bottom left corner of the difference images. Compared to nose touching experiments the increase in image quality between the zero order approach and the SENSE navigator approaches is less pronounced. The arrow points to an artifact at the posterior side of the brain that is reduced by SENSE navigator correction. Data are summarized in table 2 showing that frequency encoded and SENSE navigator correction leads to the best results.

DISCUSSION

The most important findings of this study are twofold. First, the use of sensitivity encoded and frequency encoded phase navigators leads to an improved estimation of inhomogeneous spatio-temporal magnetic field disturbances in the human brain compared to a conventional zeroth order navigator approach when strong field distortions are introduced. Second, it was shown that the image quality of heavily T_2^*-weighted acquisitions can be improved considerably by correcting for these inhomogeneities, caused primarily by patient motion outside of the imaging region.

The field map obtained during nose touching, see Figure 2 shows that the magnetic field disturbance is not homogeneous over the slice. There is a large variation between the anterior and posterior part of the brain. Consequently a global frequency estimate for the complete slice, as is obtained by a conventional zeroth order navigator, does not describe this magnetic field distribution adequately under this particular type of experiment. All the sig-

nals from the different receive coil elements that might reflect local changes, are effectively averaged in this case. Since the individual coil elements of the receive array sample only a small part of the brain, temporal changes in magnetic field can be detected and spatially resolved. If the coil elements are weighted according to their spatial sensitivity profile, low resolution spatio-temporal field change maps can be obtained, resulting in a more realistic estimation of the inhomogeneous field. When, in addition, frequency encoding of the navigator echo is used, field change estimations can be further improved. The field fluctuations introduced by nose touching are mainly oriented in the anterior-posterior direction. Therefore a frequency encoded navigator along that same direction without using coil sensitivity information already results in substantial improvements in estimating the magnetic field. In the present work significant improvements in the RSSD have been demonstrated for the SENSE and frequency encoded navigators. It should be noted that the EPI based method used to serve as a "ground truth" cannot be used for measuring magnetic field fluctuations in practical imaging studies because of the amount of time it takes to acquire the extra data. In addition the introduction of an extra RF pulse needed for the EPI readout also influences the magnetization, which is unwanted in most experiments. A navigator echo, on the other hand, can be used in a variety of imaging experiments through minor sequence adaptations. In the imaging experiments that are performed in this study, the navigator echo is acquired before the actual frequency encoding readout because of the long TE of the sequence and is part of a pre-phaser gradient already present in the sequence (see Figure 1). It does however limit the total time available for the imaging acquisition, therefore resulting in a signal-to-noise penalty. The time needed for the navigator can be minimized by sampling the navigator echo at a higher bandwidth (6) or by reducing the number of samples when no frequency encoding is required (19, 23). Due to the long imaging time needed for the EPI readout the TE_{nav} of the ground truth measurements is different from the imaging experiments

The artificially-induced changes in magnetic field distributions in this study were used to mimic (and amplify) spatio-temporal magnetic field fluctuations within a slice that have been observed in previous studies and serve as a worst case (2, 5, 6). Nose touching experiments result in substantial image degradation, as is shown in Figure 3 and 4, which result from the large variations in resonance frequency (up to 20 Hz). The image quality is considerably improved when zeroth order navigator echo correction is applied in line with previous findings in Alzheimer's disease patients using a comparable sequence (6). However, some artifacts still remain after zeroth order navigator correction, which is indicative of a spatial distribution of the magnetic field

changes that is not captured accurately using the zeroth order navigator approach. The remaining artifacts are substantially reduced when a SENSE navigator or frequency encoded navigator correction technique was employed. The best performance was observed when frequency encoding of the coil sensitivity navigator was included. The artifacts caused by deep breathing were, in general, less severe than during nose touching and the improvements between SENSE navigator correction and zeroth order correction are less pronounced. This is likely due to the relatively homogeneous magnetic field distribution that is induced by breathing for transverse slices through the brain (1, 2, 5) and smaller amplitude of the magnetic field changes (typically less than 10 Hz). In the absence of artificially introduced magnetic field fluctuations, such as nose touching or deep breathing, small image quality improvements were observed for navigator correction compared to no correction: however, no differences were found between the performance of the different navigator techniques. Another advantage of the improved navigator approaches is that the unwrapped phase images, also show fewer artifacts when correction is applied and in addition improved performance of the phase unwrapping algorithm is observed. When navigator correction is applied, artifacts arising from rapid spatial phase variations are reduced and fewer remaining phase wraps are observed. These improved phase images can be particularly helpful in applications such as susceptibility weighted imaging.

It should be noted that, in order to enable the direct comparison of the different navigator techniques the zeroth order and SENSE navigator have been acquired in a suboptimal manner in the sense that although no frequency encoding information is required, all data are actually acquired using a frequency encoding gradient followed by complex summation in the spatial-temporal or temporal domains respectively, resulting in a reduction in SNR and increased sensitivity to motion.

The concept of acquiring navigator echoes using multiple receive channels is not entirely new. Non-phase encoded free induction decay signals, similar to navigator echoes have been used in recent publications for high temporal imaging, or B_0 shimming (21–23). Others have shown that by using multi-coil navigators, improvements in image quality could be obtained by retrospectively discarding and re-measuring k-space lines that contain signal corruption exceeding a certain threshold (29). In this case the navigator echoes were acquired using a dedicated RF excitation pulse interleaved with the imaging sequence. In our approach, rather than discarding and re-measuring data, the navigator based spatial field estimations are used for retrospective ima-

ge correction and therefore require no extra scanning time. It is expected that an even higher number of elements will result in further improvements in estimating the spatial magnetic field distribution.

Methods other than navigator echoes can be used to measure dynamic magnetic field fluctuations. External field probes positioned around the subject can be used to sample dynamically magnetic field changes using free induction decay signals (11, 12). These field probes can operate at a different resonance frequency (e.g. fluorine) than the imaging sequence, limiting the interaction with the imaging sequence and therefore requiring no additional scanning time (11). However the phase changes are measured outside of the brain and data are fitted to provide the field changes within the head (11, 12), leading to a possible reduction in accuracy. Furthermore, the hardware effort needed to support these field probes is substantial potentially limiting wide applicability. An advantage of the proposed navigator approach is that the phase changes are measured *within* the brain and that no additional hardware components are necessary.

Another method to measure dynamically fluctuations in the magnetic field is to relate the phase of the respiratory cycle to a certain magnetic field distribution. A calibration scan is used to measure the magnetic field distribution at different phases of the respiration cycle using an external belt. During imaging the shim settings are adjusted according to the respiration cycle (1). However, using this approach non-periodic field changes, such as body movements, yawning and coughing cannot be corrected. Our proposed method differs in that it does not make an assumption of the periodicity or origin of the magnetic field fluctuations since it measures the field distribution for each RF excitation. Furthermore, no additional calibration scan is needed. Care needs to be taken that the echo time of the navigator (TE_{nav}) is sufficiently small such that, given the amplitude of the expected magnetic field variations, no phase wraps occur. However, for very small values of TE_{nav} the sensitivity to magnetic field variations is reduced. The maximum detectable range of magnetic field variations corresponding to TE_{nav} = 10 ms is ± 50 Hz, conservatively set to be approximately twice the estimated/observed magnetic field changes.

The proposed reconstruction framework is similar to the technique described by Liu et al. (24) in the “extreme” form where each shot comprises the acquisition of only a single k-space line. Their technique has been implemented for self-navigated sequences, such as spiral or PROPELLOR (30), whereas in our case a separate navigator echo is acquired. The approach that is used in this study incorporates the spatial sensitivity information of multiple coils

in a receive array to improve the spatial reconstruction of a magnetic field distribution map. This has been shown using a similar acquisition approach with FID navigators before, but without using the application in retrospective image correction and without using frequency encoded navigators (23). Future work will focus on implementing this method to include a frequency encoding gradient to further increase the accuracy of the dynamic field estimations. Most sequences can be modified to allow for the inclusion of a navigator echo, especially when only a limited number of points are sampled (19), whereas only certain sequences can be modified to be self-navigated. Instead of using Cartesian navigators, spiral navigators have been used to dynamically measure low resolution field maps either by self-navigation through oversampling of the center of k-space (20, 24), through the separate acquisition of a spiral navigator echo (16, 31), or orbital navigators (32). These techniques have been applied successfully in diffusion weighted imaging to correct for phase errors or in structural imaging to correct for subject motion. However in these cases the spatial dependency of the individual coil elements is not taken into account and the proposed Cartesian navigators can be acquired in a shorter amount of time, especially when no frequency encoding gradient is required.

So far, most applications of phase correction have been in the field of diffusion weighted imaging (15, 16, 20, 31) or functional imaging (13, 14, 17, 18). Both applications are very sensitive to magnetic field induced phase changes or motion. However, as was shown previously, high field (i.e. 7 Tesla) causes more sequences to be sensitive to magnetic field induced phase changes (1, 6) because the amount of phase change is directly related to the magnetic field strength. Therefore, correction for magnetic field induced phase changes becomes important also for structural imaging at high field.

In principle the proposed technique is not limited to simple gradient echo sequences, but can easily be extended to other types of data acquisition. The reconstruction framework can be used with any method that estimates dynamic field changes. Although in this study the actual imaging sequence was not accelerated by parallel imaging, the iterative image reconstruction approach is also applicable to undersampled k-space data as was shown previously (24, 33)

CONCLUSION

Changes in the magnetic field distribution in the brain, caused by physiological and/or patient motion can seriously affect high field image quality. Correcting for these artifacts is important to obtain consistent image quality

in patient studies performed at high field. By intentionally introducing strong magnetic field distortions the performance of different navigator techniques was investigated. It was found that the combination of frequency encoded navigator echoes and coil sensitivity information (SENSE navigator echoes) improved the spatial and temporal estimation of the magnetic field distribution under these exaggerated conditions, such as nose touching and deep breathing, compared to conventional zeroth order navigator estimation. Prior information about the expected direction of strongest field gradients was used for the frequency encoded techniques. Under normal conditions in cooperative subjects all investigated navigator correction approaches worked equally well.

Therefore, the proposed SENSE and frequency navigator based image correction techniques are particularly valuable in T_2^*-weighted sequences at high magnetic field strengths acquired in non-cooperative subjects.

ACKNOWLEDGMENTS

The authors thank Jorik Blaas for helpful discussions on implementing the reconstruction algorithm.

REFERENCES

1. Van Gelderen P, de Zwart JA, Starewicz P, Hinks R, Duyn JH. Real-time shimming to compensate for respiration-induced B0 fluctuations. Magnetic Resonance in Medicine 2007 ;57:362–368.
2. Van de Moortele PF, Pfeuffer J, Glover GH, Ugurbil K, Hu X. Respiration-induced B0 fluctuations and their spatial distribution in the human brain at 7 Tesla. Magnetic Resonance in Medicine 2002 ;47:888–895.
3. Raj D, Anderson AW, Gore JC. Respiratory effects in human functional magnetic resonance imaging due to bulk susceptibility changes. Physics in Medicine and Biology 2001 ;46:3331–3340.
4. Birn RM, Bandettini PA, Cox RW, Jesmanowicz A, Shaker R. Magnetic field changes in the human brain due to swallowing or speaking. Magnetic Resonance in Medicine 1998 ;40:55–60.
5. Barry RL, Williams JM, Klassen LM, Gallivan JP, Culham JC, Menon RS. Evaluation of preprocessing steps to compensate for magnetic field distortions due to body movements in BOLD fMRI. Magnetic Resonance Imaging 2010 ;28:235–244.
6. Versluis MJ, Peeters JM, van Rooden S, van der Grond J, van Buchem MA, Webb AG, van Osch MJP. Origin and reduction of motion and f0 artifacts in high resolution T2*-weighted magnetic resonance imaging: Application in Alzheimer's disease patients. NeuroImage 2010 ;51:1082–1088.
7. Conijn MMA, Geerlings MI, Luijten PR, Zwanenburg JJM, Visser F, Biessels GJ, Hendrikse J. Visualization of cerebral microbleeds with dual-echo T2*-weighted magnetic resonance imaging at 7.0 T. J. Magn. Reson. Imaging 2010 ;32:52–59.
8. Marques JP, van der Zwaag W, Granziera C, Krueger G, Gruetter R. Cerebellar Cortical Layers: In Vivo Visualization with Structural High-Field-Strength MR Imaging1. Radiology 2010 ;254:942 –948.
9. Yao B, Li T-Q, Gelderen P van, Shmueli K, de Zwart JA, Duyn JH. Susceptibility contrast in high field MRI of human brain as a function of tissue iron content. NeuroImage 2009 ;44:1259–1266.
10. Zwanenburg JJM, Versluis MJ, Luijten PR, Petridou N. Fast high resolution whole brain T2* weighted imaging using echo planar imaging at 7 T. NeuroImage 2011 ;56:1902–1907.
11. Wilm BJ, Barmet C, Pavan M, Pruessmann KP. Higher order reconstruction for MRI in the presence of spatiotemporal field perturbations. Magnetic Resonance in Medicine 2011 ;65:1690–1701.
12. Barmet C, Zanche ND, Pruessmann KP. Spatiotemporal magnetic field monitoring for MR. Magnetic Resonance in Medicine 2008 ;60:187–197.
13. Barry RL, Martyn Klassen L, Williams JM, Menon RS. Hybrid two-dimensional navigator correction: A new technique to suppress respiratory-induced physiological noise in multi-shot echo-planar functional MRI. NeuroImage 2008 ;39:1142–1150.
14. Wowk B, McIntyre M C, Saunders J K. k-space detection and correction of physiological artifacts in fMRI. Magnetic Resonance in Medicine 1997 ;38:1029–1034.
15. Anderson AW, Gore JC. Analysis and correction of motion artifacts in diffusion weighted imaging. Magn Reson Med 1994 ;32:379–387.
16. Miller KL, Pauly JM. Nonlinear phase correction for navigated diffusion imaging. Magnetic Resonance in Medicine 2003 ;50:343–353.

17. Hu X, Kim S-G. Reduction of signal fluctuation in functional MRI using navigator echoes. Magnetic Resonance in Medicine 1994 ;31:495–503.
18. Durand E, Van de Moortele PF, Pachot-Clouard M, Le Bihan D. Artifact due to B0 fluctuations in fMRI: Correction using the k-space central line. Magnetic Resonance in Medicine 2001 ;46:198–201.
19. Brau ACS, Brittain JH. Generalized self-navigated motion detection technique: Preliminary investigation in abdominal imaging. Magnetic Resonance in Medicine 2006 ;55:263–270.
20. Liu C, Bammer R, Kim D, Moseley ME. Self-navigated interleaved spiral (SNAILS): Application to high-resolution diffusion tensor imaging. Magnetic Resonance in Medicine 2004 ;52:1388–1396.
21. Lin F, Wald LL, Ahlfors SP, Hämäläinen MS, Kwong KK, Belliveau JW. Dynamic magnetic resonance inverse imaging of human brain function. Magnetic Resonance in Medicine 2006 ;56:787–802.
22. Hennig J, Zhong K, Speck O. MR-Encephalography: Fast multi-channel monitoring of brain physiology with magnetic resonance. NeuroImage 2007 ;34:212–219.
23. Splitthoff DN, Zaitsev M. SENSE shimming (SSH): A fast approach for determining B0 field inhomogeneities using sensitivity coding. Magn. Reson. Med. 2009 ;62:1319–1325.
24. Liu C, Moseley ME, Bammer R. Simultaneous phase correction and SENSE reconstruction for navigated multi-shot DWI with non-cartesian k-space sampling. Magnetic Resonance in Medicine 2005 ;54:1412–1422.
25. Sutton BP, Noll DC, Fessler JA. Fast, iterative image reconstruction for MRI in the presence of field inhomogeneities. IEEE Trans Med Imaging 2003 ;22:178–188.
26. Fong D, Saunders M. LSMR: An iterative algorithm for sparse least-squares problems [Internet]. arXiv:1006.0758 2010 ;
27. Roemer PB, Edelstein WA, Hayes CE, Souza SP, Mueller OM. The NMR phased array. Magn Reson Med 1990 ;16:192–225.
28. Rauscher A, Barth M, Herrmann K-H, Witoszynskyj S, Deistung A, Reichenbach Jã¼R. Improved elimination of phase effects from background field inhomogeneities for susceptibility weighted imaging at high magnetic field strengths. Magnetic Resonance Imaging 2008 ;26:1145–1151.
29. Kober T, Marques JP, Gruetter R, Krueger G. Head motion detection using FID navigators. Magnetic Resonance in Medicine 2011 ;66:135–143.
30. Pipe JG, Farthing VG, Forbes KP. Multishot diffusion-weighted FSE using PROPELLER MRI. Magn Reson Med 2002 ;47:42–52.
31. Van A, Hernando D, Sutton B. Motion-Induced Phase Error Estimation and Correction for 3D Diffusion Tensor Imaging [Internet]. IEEE Trans Med Imaging 2011 ;
32. Moriguchi H, Lewin JS, Duerk JL. Novel interleaved spiral imaging motion correction technique using orbital navigators. Magnetic Resonance in Medicine 2003 ;50:423–428.
33. Pruessmann KP, Weiger M, Börnert P, Boesiger P. Advances in sensitivity encoding with arbitrary k-space trajectories. Magnetic Resonance in Medicine 2001 ;46:638–651.